Label-free detection and enumeration of *Giardia* cysts in agitated suspensions using *in situ* microscopy

Valdinei L. Belini[a*], Natália de Melo Nasser Fava[b], Lucas Ariel Totaro Garcia[c], Maria Júlia Rodrigues da Cunha[d], Lyda Patrícia Sabogal-Paz[e]

[a] Valdinei L. Belini ([*]Corresponding author)

Department of Electrical Engineering, Universidade Federal de São Carlos, Rodovia Washington Luís, km 235, São Carlos-SP, CEP 13565–905, Brazil

Phone: +55 (16) 3306–6618, Fax: +55 (16) 3351–9701

E-mail: belini@ufscar.br

[b] Natália de Melo Nasser Fava

Department of Hydraulics and Sanitation, São Carlos School of Engineering, University of São Paulo, Avenida Trabalhador São-Carlense, 400. São Carlos-SP, CEP 13566-590, Brazil

[c] Lucas Ariel Totaro Garcia

Department of Hydraulics and Sanitation, São Carlos School of Engineering, University of São Paulo, Avenida Trabalhador São-Carlense, 400. São Carlos-SP, CEP 13566-590, Brazil

[d] Maria Júlia Rodrigues da Cunha

Department of Hydraulics and Sanitation, São Carlos School of Engineering, University of São Paulo, Avenida Trabalhador São-Carlense, 400. São Carlos-SP, CEP 13566-590, Brazil

[e] Lyda Patrícia Sabogal-Paz

Department of Hydraulics and Sanitation, São Carlos School of Engineering, University of São Paulo, Avenida Trabalhador São-Carlense, 400. São Carlos-SP, CEP 13566-590, Brazil

Abstract

Laboratory procedures performed in water treatment studies frequently require the characterization of (oo)cyst suspensions. Standard methods commonly used are laborious, expensive and time-consuming, besides requiring well-trained personnel to prepare samples with fluorescent staining and perform analysis under fluorescence microscopy. In this study, an easy cost-effective *in situ* microscope was assessed to acquire images of *Giardia* cysts directly from agitated suspensions without using any chemical labels or sample preparation steps. An image analysis algorithm analyzes the acquired images, and automatically enumerates and provides morphological information of cysts within 10 min. The proposed system was evaluated at different cyst concentrations, achieving a limit of detection of ~30 cysts/mL. The proposed system overcomes cost, time and labor demands by standard methods and has the potential to be an alternative technique for the characterization of *Giardia* cyst suspensions in resource-limited facilities, since it is independent of experts and free of consumables.

Keywords: Water quality, Parasites, Protozoa, USEPA, *Giardia*, Computer

1. INTRODUCTION

Giardia is an environmentally ubiquitous enteropathogen distributed worldwide, which has a simple life cycle with two main stages, the proliferating trophozoite in the small intestine and the infectious cysts that are spread most often via contaminated water (Einarsson et al., 2016). This protozoan has previously been associated with several gastrointestinal waterborne outbreaks, especially in developed countries, being responsible for 280 million gastrointestinal infections (Thompson et al., 2005; Ankarklev et al., 2010), which makes *Giardia* spp. a public health risk and an important target in environmental research and sanitation (Rosado-Garcia et al., 2017).

Current methods for detecting protozoa in water samples, such as the Environmental Protection Agency (EPA) 1623 (USEPA, 2012), rely on concentration, immunomagnetic separation of cysts from debris, and staining with specific fluorescent dyes, followed by cyst detection and counting by a manual process on laboratory fluorescence microscopes. These methods are laborious, time-consuming, need bulky and expensive equipment, and well-trained personnel to operate the microscope and perform analysis.

Only a few detection approaches compatible with field instrumentation have been described to detect and count *Giardia* cysts in water samples. Commonly used approaches to evaluate the microbial water quality using smartphone-based microscopy (Shrestha et al., 2020; Koydemir et al., 2015) and portable imaging flow cytometer (Göröcs et al., 2020) require, respectively, fluorescent reagents specific for *Giardia* cysts and disposable components (*e.g.*, plastic tubing and sample channel) for each measurement. This partially hinders their use in low-resource settings including remote and field sites when waterborne monitoring is needed on a more frequent basis.

In situ microscopy (Suhr et al., 1995) is an alternative technique enabling one to overcome the aforementioned constraints. Its principle allows qualitative and quantitative

characterization of cells and particles suspended in a liquid medium and has been used to monitor the cell number, cell size distribution, and morphological characteristics of several specimens, including yeasts (Belini et al., 2020; Belini et al., 2017; Marquard et al., 2016; Lindner et al., 2007; Wei et al., 2007; Brückerhoff et al., 2005; Camisard et al., 2002; Frerichs et al., 2001; Bittner et al., 1998; Suhr et al., 1995), Chinese hamster ovary cells (Lüder et al., 2014), and the viability of mammalian cells (Wiedemann et al., 2011). The imaging performance of the *in situ* microscopy has already been evaluated in wastewater for the morphological characterization of filamentous bacteria (Dias et al., 2016; Dunkel et al., 2016).

To the best of our knowledge, no study has been carried out using *in situ* microscopy to acquire microscopic images of unstained *Giardia* cysts. Based on this, we aimed to assess the potential of this technology in conjunction with image analysis algorithms to automatically detect and enumerate *Giardia* cysts in agitated suspensions without the need for any chemical labels, sampling chamber replacement, or sample concentration.

2. MATERIALS AND METHODS

2.1 Preparation of *Giardia* cyst suspensions

To obtain the suspensions for the *in situ* experiments, 1 mL standard *Giardia* spp. cyst suspension (Waterborne™, Inc., New Orleans, LA, USA) containing ~10^5 cysts was homogenized for 2 min in vortex and vigorously pipetted 20 times, and used as the stock suspension. Afterwards, this suspension was serially diluted with distilled water. For each suspension, aliquots of 50 µL were prepared with a Merifluor® (Meridian Bioscience, Inc.) kit according to the manufacturer's recommendations and Method 1623.1 (USEPA, 2012), and the number of cysts was measured in duplicate on a fluorescence microscopy (BX51, Olympus®, $\lambda_{excitation}$ = 475 nm, $\lambda_{emission}$ = 520 nm). From this process, average concentrations of *Giardia*

were obtained at 30, 50, 250, 510 cysts/mL. A negative control was also prepared using 1 mL of diluted cyst-free water.

2.2 Image acquisition

A high-resolution (~0.3 µm) *in situ* microscope (Suhr et al., 1991) was built and used to acquire microscopic images directly from *Giardia* cysts suspensions. A photograph of the imaging system is shown in Fig. 1.

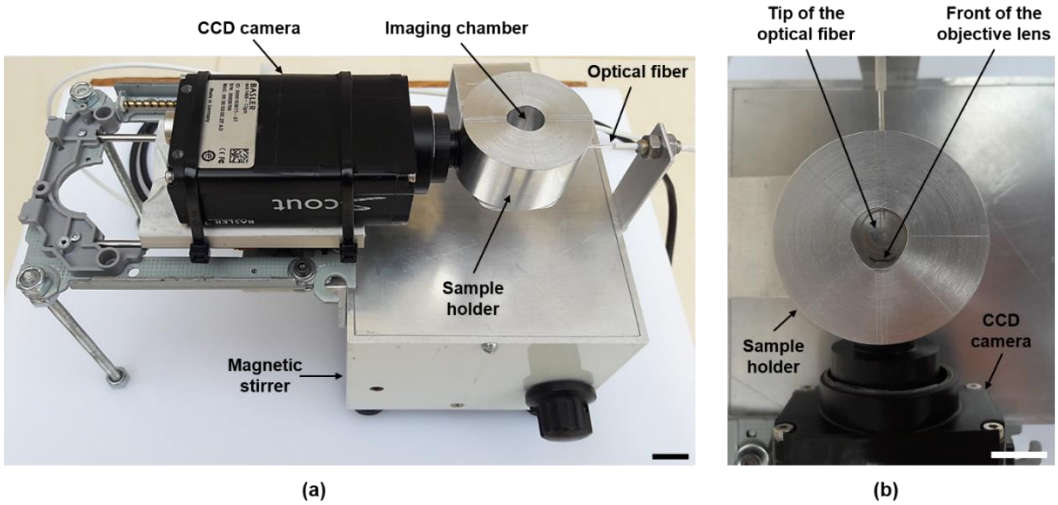

Fig. 1. Photograph of the *in situ* microscopy-based system for label-free detection and enumeration of *Giardia* cysts directly from water samples. (a) Perspective view of the whole system. (b) Top view of the sample holder. The sampling container equipped with the *in situ* microscope was designed to have a working volume of 1.5 mL, which is 30-fold larger than the volume of aliquots commonly analyzed using standard methods under fluorescence microscopy. The magnetic bar (2 × 2 × 5 mm) inside the imaging chamber is not shown. Scale bar = 1 cm.

Essentially, the *in situ* microscope (ISM) consists of a transmitted brightfield microscope that is directly coupled to moving suspensions to capture micrographs of the suspended cells and particles. The 1.5 mL working volume container was machined from an

aluminum block and equipped with the ISM and inoculated with 1 mL cyst suspension for the *in situ* experiments.

The LED (DieMOUNT, Wernigerode, Germany) peak-wavelength at 650 nm, nominally 4 mW at 20 mA, peak current approximately 2 A, pulse-length 0.5–10 µs, was used for illumination. An optical fiber pigtail was used to guide light to provide direct light microscopy. The micrographs were acquired by a digital camera (SCA1400–17 gm, Basler, Ahrensburg, Germany, CCD-size 8.98 mm × 6.71 mm, 1392 × 1040 pixels, pixel size 6.45 × 6.45 μm^2, bitmap, 8 bits) through a solid immersion lens-objective (20×, NA = 0.75). The latter was designed and characterized by Suhr & Herkommer (2015).

In order to avoid cross-contamination between measurements for different cyst concentrations, the imaging container was systematically cleaned. Before the *in situ* experiments, a first cleaning procedure was performed ~30 times, until no more objects were visualized in the real-time Graphical User Interface of the image acquisition system. The cleaning process involved vigorous pipetting of cyst-free distilled water into the container and subsequently sucking out the whole water volume from the container. The cleaning procedure was also performed three times between each measurement.

The image acquisition parameters such as light pulse width, camera gain, and exposure time, were all set up once at the beginning of the study and remained unchanged throughout the experiment.

For the *in situ* experiments, the container was inoculated with 1 mL of suspension, and a magnetic stirrer (~150 rpm) was used for agitation. Microscopic images were acquired immediately after the cyst suspensions were inoculated into the imaging container.

2.3 Image analysis

An image analysis algorithm was implemented using the MATLAB Image Processing Toolbox in an Intel PC, Quad-CPU, 2.66 GHz, 4.0 GB RAM. As shown in Fig. 2, the algorithm

comprises two main sections: (*i*) detection of objects from ISM images followed by portrait generation, and (*ii*) feature extraction followed by cyst classification.

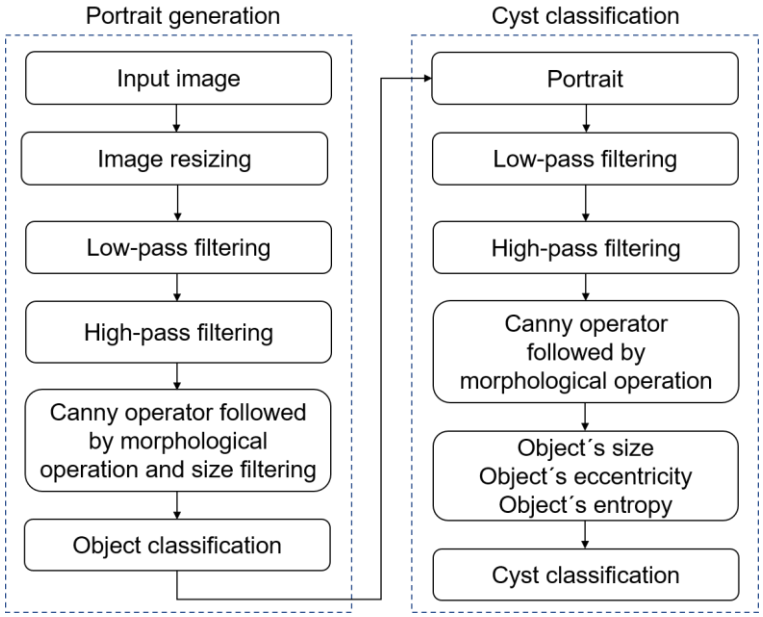

Fig. 2. Flowchart of all operations performed to generate portraits containing *candidate* objects and to perform classification for each detected object.

2.3.1 Object detection

The first step is to detect objects from the ISM image to create portraits containing a single object. Due to the sparse images, a large number of images was needed to capture a single cyst. In order to optimize the algorithm with respect to computational time, it was essential to first reduce the original image resolution (1392 × 1040 pixels) by a factor of four, resulting in 348 × 260 pixels images. Prior to detecting objects in the acquired images, the following image preprocessing steps were performed: first, a noise reduction step was carried out using a 5 × 5 median filter (Gonzalez & Woods, 2008) to reduce high-frequency noises. Afterwards, a high-pass filter (disk-shaped, 2 pixels) was applied in the smoothed image to sharpen the objects´ border. To find objects in the processed image, the Canny operation was computed (Gonzalez & Woods, 2008) to create a binary image containing closed lines of connected white pixels on a black background. Short gaps in the lines of pixels are closed by a morphological dilation

operation (Gonzalez & Woods, 2008) using 2-pixel line structuring elements followed by hole filling and border image cleaning. Afterwards, the shape of the object is further smoothed by applying morphological opening operation (Gonzalez & Woods, 2008) in the resulting binary image. Detected objects in the reduced image, which have sizes not within the range of values expected for cysts (100 – 210 pixels), are discarded by size filtering.

This first step of the algorithm only performs a preliminary segmentation of objects from the background to localize them and generate portraits containing detected objects. Only in these portraits are the detected objects evaluated and classified by the algorithm as *candidate* cysts. As the analyzed water samples contain a diversity of objects exhibiting a variety of sizes and shapes, their influence on the image analysis is minimized by detecting only regularly shaped objects. This selection is made by computing the *solidity factor* (Soltys et al., 2005) of each object. This is a scalar that specifies the proportion of pixels in the convex hull that are also inside the detected object. By applying a threshold value (0.90) for the solidity factor of every binary object, irregularly shaped structures are discarded.

From the final binary image, the centroid of the pre-classified objects is determined, and this information is used to crop corresponding portraits (70 × 70 pixels) from the original (unreduced) ISM image.

2.3.2 Feature extraction

Once the objects are successfully detected using the steps described above, the classification of objects contained in the portraits as cysts or non-cysts is carried out by performing the operations shown in Fig. 2. First, a noise reduction step is carried out in the portrait cropped from the original ISM image using a 5 × 5 median filter (Gonzalez & Woods, 2008) to reduce high-frequency noises. Afterwards, a high-pass filter (disk-shaped, 3 pixels) is applied in the smoothed image to sharpen the objects´ border. To find objects in the processed image, the Canny operation was computed (Gonzalez & Woods, 2008) to create a binary image containing

closed lines of connected white pixels on a black background. Short gaps in the lines of pixels are closed by a morphological closing operation (Gonzalez & Woods, 2008) using 4-pixel disk structuring elements followed by hole filling and selection of the largest object contained inside the portrait.

Afterwards, the size of the object is determined as the number of pixels forming it. This information is used to identify only those objects that have sizes within the range of values expected for cysts in the unreduced image.

Due to the typical elliptical shape of the cysts, this feature was parameterized by the eccentricity of the ellipse that has the same second moments as the region under analysis (MathWorks™, 2021):

$$Eccentricity = \frac{Distance\ between\ the\ foci\ of\ the\ ellipse}{Major\ axis\ length} \quad (1)$$

where the *major axis length* is the length (in pixels) of the major axis of the ellipse that has the same normalized second central moments as the region. A null eccentricity designates a perfect circle, while values increasing towards 0.5 describe shapes increasingly more elliptical, and unitary eccentricity describes a line segment. By applying a threshold value for the eccentricity factor of every binary object, irregularly shaped structures can be discarded from further analysis by the algorithm.

As portraits containing naturally existing micro-objects in sample water, whose shapes and sizes could resemble those of cysts, may still remain after applying the two above-computed parameters, the completeness for cyst classification involves the computation of their inhomogeneity. Following the image evaluation steps described by Wiedemann et al. (2011), the average local entropy was computed for each original (unreduced) grayscale portrait as a measure of inhomogeneity. To confine the computation of the entropy inside the object, firstly the object boundary, as determined by the algorithm, was used to define the region of interest

(ROI) in which the entropy is computed. Afterwards, for each pixel inside this region, the local entropy *E* in the pixel´s 3 × 3 neighborhood is computed (Gonzalez & Woods, 2008):

$$E = -\sum P(i).log_2[P(i)] \quad bits \tag{2}$$

where *i* runs over all gray values occurring in the 3 × 3 pixels neighborhoods. Finally, the mean value of all local entropies in the ROI is computed as a measure of inhomogeneity of the object.

In addition, the length and the width of the cysts was determined as the maximum and minimum Feret´s diameters (MathWorks™, 2021), respectively. Each imaged pixel corresponds to a real dimension given by the pixel size over optical magnification:

$$Length\ represented\ by\ one\ pixel = \frac{6.45\ \mu m}{20} = 0.32\ \mu m \tag{3}$$

2.3.3 Object classification

It was observed in the experiments that the cyst sizes were typically in a narrower range of values (~900 – 1400 pixels) compared to other micro-objects contained in the analyzed water samples. This information was used as one of the criteria for cyst classification. In logical AND in conjunction with this criterion, a narrow range of values (~0.60 – 0.86) for the eccentricity factor was used. An interval of inhomogeneity inside the ROI (~050 – 0.83 bits), measured as entropy, was used as a third criterion in logical AND conjunction with the two other criteria. Since objects having size, inhomogeneity, and eccentricity values within the range of those expected for cysts, may be falsely classified as cysts, the maximum pixel intensity (> 250) inside the ROI was also used as a classification criterium in logical AND conjunction with the three other criteria.

2.4 Performance evaluation

Each object portrait was visually inspected to evaluate the performance of the algorithm. Regarding cyst classification, the algorithm´s outcome was manually classified as true positive (*TP*), false positive (*FP*), false negative (*FN*), or true negative (*TN*), defined as follows:

complete cyst bodies, the largest fragment of over-segmented cysts (*i.e.*, cysts divided into many parts), and one cyst for each case of under-segmentation (*i.e.*, cysts agglomerates segmented as one cyst) are classified as *TP*. Halo artifacts and intensity irregularities in the image background are classified as *FP*. Missed cysts and remaining cysts in cases of under-segmentation are classified as *FN*. The listed terms were adapted from Buggenthin et al. (2013).

Finally, the sensitivity (*SE*), precision (*PR*), and accuracy (*ACC*) values are computed to quantitatively evaluate the performance of the algorithm (Buggenthin et al., 2013):

$$SE = \frac{TP}{TP + FN} \tag{4}$$

$$PR = \frac{TP}{TP + FP} \tag{5}$$

$$ACC = \frac{TP}{TP + FN + FP} \tag{6}$$

3. RESULTS AND DISCUSSION

3.1 Detection of objects within ISM images

Figure 3 shows examples of portraits of cysts captured by the *in situ* microscope at suspensions containing different cyst concentrations.

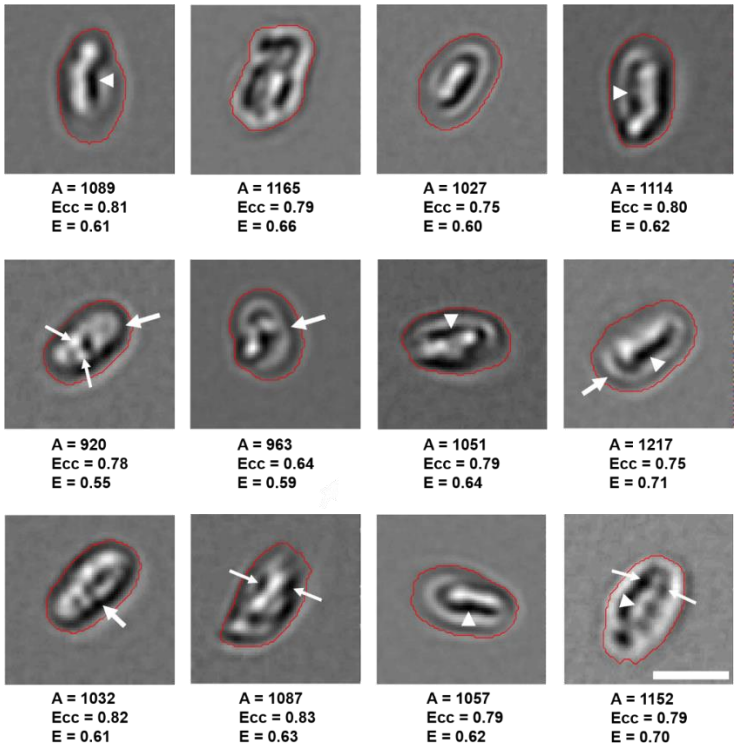

Fig. 3. Examples of *in situ* microscopy cyst-portraits acquired directly from the suspension using the proposed system. Thick arrow points to cyst wall (Al Saad & Al Emarah, 2014). Thin arrow and arrowhead point to structures that resemble nuclei and axoneme, respectively. The red line depicts the object contour as determined by the algorithm for determining size and shape and also indicates the region of interest inside which the local entropy was computed. The corresponding values represent the size in pixels, the eccentricity, and the mean entropy (in bits). Scale bar = 10 µm.

As shown in Fig. 3, the detected cysts exhibit a moderate range of sizes and inhomogeneities with respect to the intracellular content. In common with most detected cysts is their regular elliptical-like shape. It can be seen that the more regular cysts in shape (elliptical) are more homogeneous with respect to size and intracellular content and slightly smaller than non-elliptical cysts.

In-focus, slightly over-focused (*i.e.*, cysts located between the light source and the focal plane generating smooth dark edges and cyst content brighter than the rest of the cyst) and

slightly under-focused cysts (*i.e.*, cysts located between the objective lens and the focal plane appearing as slightly dark and blurred structures, as shown in the last row and column in Fig. 3), were captured. More complex textures inside cysts can be observed when they are in-focus (Fig. 3). The occurrence of these different focusing conditions poses extra challenges to the cyst detection stage with fixed parameters such as the threshold values and the cut-off frequencies in the filters. To tune the algorithm´s parameters, we prioritized minimizing the likelihood of false positives as misclassifying water samples would make the whole water sample under analysis positive (false) for *Giardia* contamination, as inspired by Göröcs et al. (2020). These parameters were optimized once by experiment and kept constant during the whole study.

Besides single cysts and some internal structures, the ISM also captured the diversity of other possible micro-objects contained in the analyzed water samples and that of cyst configurations (Fig. 4).

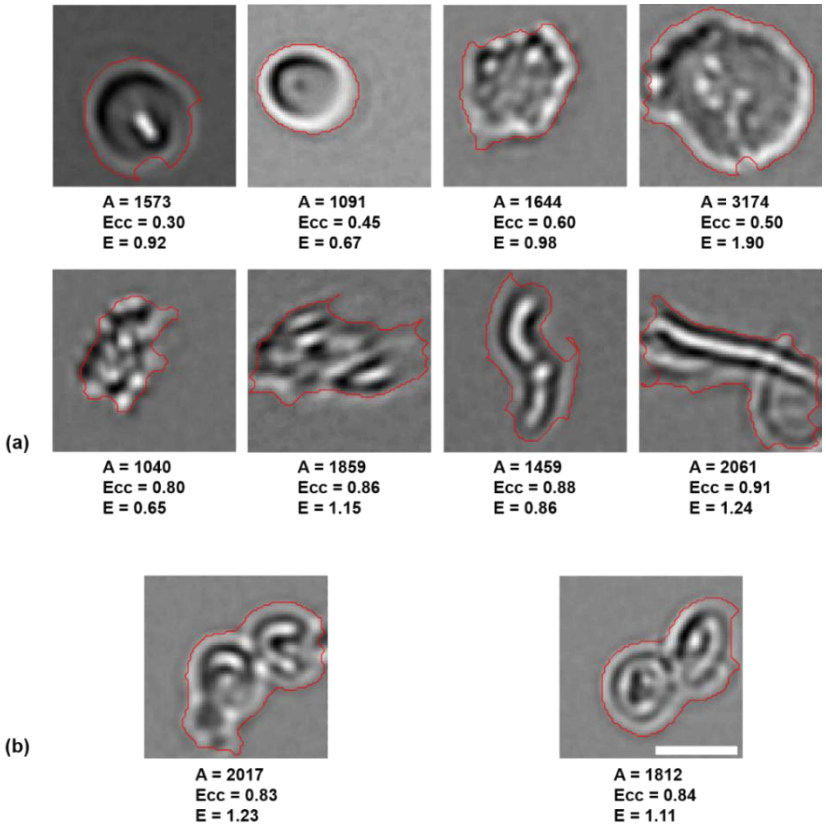

Fig. 4. Examples of different non-cyst particles and cyst agglomerates from ISM images. (a) The first two objects from left to right in the first row are probably gas bubbles. The objects in the other portraits could not be identified. (b) Cyst agglomerates. The red line depicts the object contour as determined by the algorithm for determining size and shape and also indicates the region of interest inside which the local entropy was computed. The corresponding values represent the size in pixels, the eccentricity, and the mean entropy in bits. Scale bar = 10 μm. All portraits share the same scale bar.

As shown in Fig. 4, contaminating particles having size and shape heterogeneity and inhomogeneity regarding the internal content were also acquired by the ISM. However, these particles were not classified as cysts by the algorithm. When compared to typical values for size, eccentricity factor, and mean entropy (Fig. 3), cysts can be easily distinguished from non-cyst particles. More oblong objects (most resembling *Giardia* cysts) were selected by using the eccentricity index, while the attribute size helped exclude objects with sizes not within the range of values expected for cysts. Finally, the two latter parameters in logical AND combination with the mean entropy, computed in the region of interest inside the object´s boundary, as determined by the algorithm, eliminated objects morphologically similar to cysts (Fig. 4).

In addition to the counting, the cysts were also characterized with respect to their dimensions by the proposed system, which is not available using standard methods. From the image analysis computed in the classified portraits, *Giardia* cysts are most elliptical-shaped objects having an average length and width of 16.37 ± 1.76 μm and 11.13 ± 1.63 μm, respectively. Since the observed cyst agglomerates are much larger than single cysts (Fig. 4b), they were excluded from the computation of the dimensions. The computed dimensions are consistent with those reported elsewhere for *Giardia* spp. cysts (Efstratious et al., 2017; Karanis et al., 2007; Filice et al., 1952).

The acquired images were analyzed using size, shape, and texture-based thresholding for the elimination of contaminating particles and morphologically similar objects to the cysts, as well as for the isolation of strongly out-of-focus particles. Despite the diversity of non-cyst particles (Fig. 4), standard operations of image processing (Gonzalez & Woods, 2008) were sufficient to detect and enumerate *Giardia* cysts directly from suspensions. Different from using machine learning algorithms to analyze dozens of extracted parameters derived to characterize *Giardia* cysts (Koydemir et al., 2015) or using complex deep-based neural networks requiring experts and time-consuming training steps (*e.g.*, Göröcs et al., 2020), the proposed algorithm combines only standard techniques of digital image processing, making it much simpler, intuitive, easy-to-use, reliable, and reproducible with any common image evaluation software package on a standard computer.

Each cyst concentration was documented with ~4500 ISM images acquired at a rate of 15 images per second, totalizing ~5 min for image acquisition plus ~5 min for image analysis. The analysis of the data for the five concentrations resulted in the relationship between the ISM signal and counts under fluorescence microscopy shown in Fig. 5.

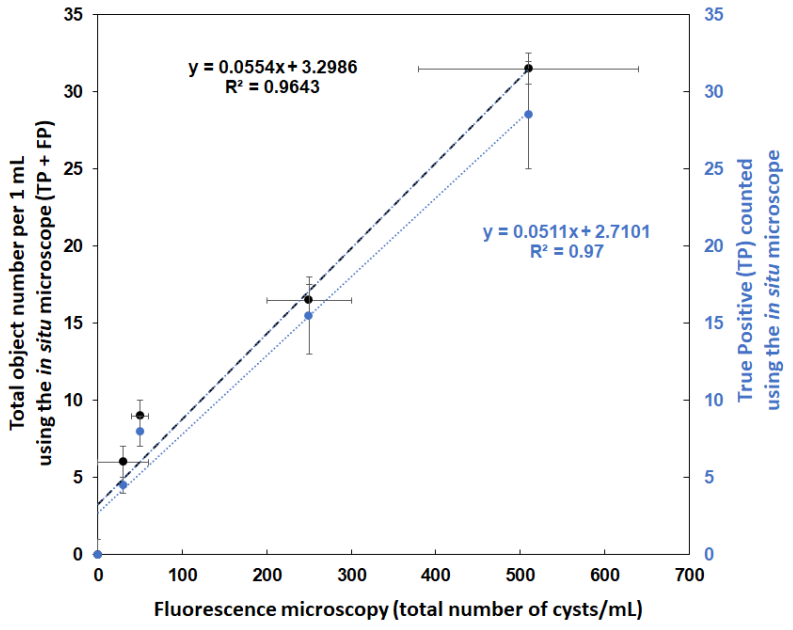

Fig. 5. Correlation between the total cyst count using the proposed system and the manual cyst count using the standard method. For each concentration, duplicate measurements were made by both the proposed method and manual counting. The solid dots represent the experimental data points. The vertical and horizontal error bars denote the standard deviation for the proposed and manual method, respectively. The data point null for both data sets is shown in blue. The correlation coefficients are also shown.

The results show a satisfactory relationship (R^2 = 0.97) between cysts counted by the proposed system and manual count in the range 0 – 510 cysts/mL, as assessed by fluorescence microscopy according to the standard method.

In Fig. 5, the achieved limit of detection (LoD) is 30 cysts/mL. This value is much lower than that using lens free microscopy (~190 cysts/mL; Mudanyali et al., 2010), but significantly larger than those by other imaging-based approaches involving holographic microscopy (~0.4 cysts/mL; Göröcs et al., 2020) and smartphone-based microscopy in samples prepared with Lugols´ iodine (~0.7/mL derived from reported 73 cysts/100 g; Shrestha et al., 2020) or fluorescent dyes (~1.2 cysts/mL; Koydemir et al., 2015). However, the proposed system is also fast and does not require sample concentration steps, inputs and/or disposable components. Thus, it is independent of experts to prepare samples and dedicated sampling devices, which make sample preparation difficult and discourage the use of mobile platforms in field analysis for pathogen detection (Wu et al., 2017). Based on the imaging performance of the built ISM, this LoD might be improved by acquiring larger numbers of images in cyst concentrations one order of magnitude lower, at the expense of larger times for image acquisition and analysis. Alternatively, similar to observations by other authors (*e.g.*, Mudanyali et al., 2010), the usage of sample concentration methods such as centrifugation and filtering (Fava et al., 2021; Franco et al., 2016; USEPA, 2012) might further improve the detection limit by a factor of ~100-fold to claim a detection sensitivity of ~0.3 cyst/mL.

The literature describes *Giardia* cyst concentration in raw water that are several orders of magnitude below those used in the work described (Efstratiou et al., 2017). At the current state presented here, we propose to apply the proposed system for the characterization of *Giardia* cyst suspensions commonly used, *e.g.*, in water treatment studies in laboratory-scale experiments (Adeyemo et al., 2015; Fava et al., 2021; Franco et al., 2016; Freitas et al., 2021). Since this system requires neither reagents nor sample preparation steps, its application to rapidly enumerate *Giardia* cysts in an automated process would reduce detection time, reduce the level of human intervention required, and contribute to the saving of resources (McGrath et al., 2017). With slight modifications in the image analysis algorithm aiming to cope with larger numbers and diversity of other particles, this system has the potential to be used for the detection of cysts in high-concentration suspensions in water treatment plants with operating problem or in those that adopt the recirculation of the filter backwash water (Karanis et al., 1996), which may be responsible for an increased risk of reinserting large amount of (oo)cysts into the system (Freitas et al., 2010).

As a matter of fact, the *in situ* microscopy-based system proposed herein has significant advantages over other imaging-based approaches. First, its real-time imaging system enables direct screening of water samples, since no processing steps are needed to visually localize and reconstruct the particles present in the liquid volume as in the case of holographic microscopy (Göröcs et al., 2020). Second, in terms of application in resource-limited settings, the field-portable design of the proposed system is quite advantageous as it requires neither disposable components (Göröcs et al., 2020) nor fluorescent labeling (Koydemir et al., 2015), in which the latter further complicates sample preparation and discourages mobile platforms from the field testing of pathogen detection (Wu et al., 2017). In regions with limited infrastructure, a ready-to-use system such as the one proposed here could benefit laboratory personnel in terms of the ability of characterizing *Giardia* cyst suspensions in a few minutes, with the added advantage of not requiring specialists to prepare samples or replace sampling devices. In addition, the

sub-micrometric optical resolution (~0.3 µm) of the solid immersion-based objective *in situ* microscope (Suhr & Herkommer, 2015) enables detecting even smaller waterborne pathogens, such as *Cryptosporidium* oocysts, which also present a major health challenge globally (Göröcs et al., 2020).

3.2 Performance evaluation of the proposed method

The overall performance of the cyst segmentation algorithm was evaluated by comparing its outcome with portraits inspected manually. The results are summarized in Table 1.

Table 1. Performance evaluation of the algorithm. The average number of cysts, as determined in duplicate by both algorithm and standard methods, is shown as the mean ± SD. On average, 98 ± 14, 81 ± 5, 239 ± 67, and 412 ± 18 portraits were segmented by the algorithm, and then examined manually for the concentrations of 30, 50, 250, and 510 cysts/mL, respectively.

	Concentration (cysts/mL)[a]			
Parameter	**510**	**250**	**50**	**30**
Total number of cysts by manual inspection	28.5 ± 3.5	15.5 ± 2.5	8.0 ± 1.0	4.5 ± 0.5
Total number of cysts by proposed system	31.5 ± 3.5	16.5 ± 3.5	9.0 ± 0.0	6.0 ± 0.0
True positives	28.5	15.5	8.0	4.5
False positives	3.0	1.0	1.0	1.5
False negatives	4.5	2.5	0.5	0.0
Sensitivity	0.87 ± 0.05	0.86 ± 0.04	0.95 ± 0.05	1.00 ± 0.00
Precision	0.92 ± 0.01	0.95 ± 0.05	1.00 ± 0.00	0.83 ± 0.17
Accuracy	0.80 ± 0.04	0.82 ± 0.00	0.84 ± 0.06	0.75 ± 0.08

[a] *Giardia* cyst concentration based on fluorescence microscopy.

The image analysis performance described by an average sensitivity (92%), precision (93%), and accuracy (80%) shows that the algorithm performed satisfactorily well by applying the same classification strategy with fixed values for all algorithm´s parameters regardless of cyst concentration. Most misclassifications were observed in images of cysts acquired under different imaging conditions. Specifically, missing cysts (*i.e.*, *FN* cases) occurred for poorly contrasted cysts. The few *FP* cases were caused mainly by objects having parameters with

values within those expected for cysts. The occurrence of cysts agglomerates was observed in the two highest concentrations. In these cases, one two-agglomerate cysts (Fig. 4b, *left*) and one three-agglomerate cysts (Fig. 4b, *right*) were correctly classified as containing two cysts each on the basis of its 2-fold size larger than the average size for single cysts, in conjunction with the other regular criteria for cyst classification adjusted for agglomerate detection. In the latter case, however, one cyst was missed due to its poorer contrast compared to the neighbor cysts in the same agglomerate (Fig. 4b, *right*).

4. CONCLUSIONS

This paper proposed using *in situ* microscopy in conjunction with image analysis algorithms for detecting and enumerating unstained *Giardia* cysts directly from agitated suspensions. The automatic counting results were compared to manual counting from standard methods, showing satisfactory performance at different cyst concentrations. Besides to a rapid quantification, the proposed system also provided in a short time information related to the morphology of the cysts, without requiring chemical labels or sample concentration steps. The results presented herein, provide subsidies for the improvement of the technology, so that it can, in the near future, become a simple, ready-to-use, and reliable method for the detection of *Giardia* cyst, and/or other pathogens, in field or laboratory experiments, demanding less effort and reduced cost when compared to standard detection methods, given that the presented system is automatic and free of consumables.

Acknowledgments

The authors would like to thank Prof. Hajo Suhr, Department of Information Technology of Mannheim University of Applied Sciences, Mannheim, Germany, for kindly providing the camera, electronic hardware, image acquisition software, and the lenses and mechanical mounting of the objective.

CRediT author statement

Valdinei Luís Belini: Conceptualization, Methodology, Software, Investigation, Validation, Writing-Original Draft & Editing**. Natália de Melo Nasser Fava:** Methodology, Investigation, Writing-Original Draft. **Lucas Ariel Totaro Garcia**: Methodology, Writing-Original Draft. **Maria Júlia Rodrigues da Cunha:** Methodology, Writing-Original Draft. **Lyda Patricia Sabogal Paz:** Funding acquisition, Project administration, Conceptualization, Writing-Review & Editing.

Data and code availability

The datasets generated during the current study and the developed code are available from the corresponding author on reasonable request.

Funding

This work was partially supported by The Royal Society (ICA\R1\201373 - International Collaboration Awards 2020) and National Council for Scientific and Technological Development (CNPq 308070/2021-6).

Competing interests

The authors have no competing interests to declare that are relevant to the content of this article.

References

Adeyemo, F. E., Kamika, I., Momba, M. N. B. 2015. Comparing the effectiveness of five low-cost home water treatment devices for *Cryptosporidium*, *Giardia* and somatic coliphages removal from water sources. Desalin. Water Treat., 56(9), 2351-2367.

Al Saad, R. K., Al Emarah, G. Y. 2014. Morphological descriptive study of *giardia lamblia* in man and cow at basrah. International Journal of Biological Research, 2(2), 125-128.

Ankarklev, J., Jerlström-Hultqvist, J., Ringqvist, E., Troell, K., Svärd, S. G. 2010. Behind the smile: cell biology and disease mechanisms of *Giardia* species. Nat. Rev. Microbiol., 8, 413-422.

Belini, V. L., Suhr, H., Wiedemann, P. 2020. Online monitoring of the morphology of an industrial sugarcane biofuel yeast strain *via in situ* microscopy. J. Microbiol. Methods, 175, 105973.

Belini, V. L., Caurin, G. A. P., Wiedemann, P., Suhr, H. 2017. Yeast fermentation of sugarcane for ethanol production: Can it be monitored by using *in situ* microscopy? Braz. J. Chem. Eng., 34(4), 949-959.

Bittner, C., Wehnert, G., Scheper, T. 1998. *In situ* microscopy for on-line determination of biomass. Biotechnol. Bioeng., 60, 24–35.

Brückerhoff, T., Frerichs, J. G., Joeris, K., Konstantinov, K., Scheper, T. 2005. Animal cell technology meets genomics. In: Godia F., Fussenegger M. (eds), Proceedings of the 18th ESACT Meeting. Springer, Spain, pp. 589-592.

Buggenthin, F., Marr, C., Schwarzfischer, M., Hoppe, P. S., Hilsenbeck, O., Schroeder, T., Theis, F. J. 2013. An automatic method for robust and fast cell detection in bright field images from high-throughput microscopy. BMC Bioinform., 14, 297.

Camisard, V., Brienne, J. P., Cassar, J. Ph., Hammann, J., Suhr, H. 2002. Inline Characterization of cell-concentration and cell-volume in agitated bioreactors using *in situ* microscopy: application to volume variation induced by osmotic stress. Biotechnol. Bioeng., 78, 73-80.

Dias, P. A., Dunkel, T., Fajado, D. A., Gallegos, Ede L., Denecke, M., Wiedemann, P., Schneider, F. K., Suhr, H. 2016. Image processing for identification and quantification of filamentous bacteria in *in situ* acquired images. Biomed. Eng. Online, 15, 64.

Dunkel, T., Dias, P. A., de León Gallegos, E. L., Tacke, V., Schielke, A., Hesse, T., Fajado, D. A., Suhr, H., Wiedemann, P., Denecke, M. 2016. *In situ* microscopy as a tool for the

monitoring of filamentous bacteria: a case study in an industrial activated sludge system dominated by *M. parvicella*. Water Sci. Technol., 73, 1333-1340.

Efstratiou, A., Ongerth, J., Karanis, P. 2017. Evolution of monitoring for *Giardia* and *Cryptosporidium* in water. Water Res., 123, 96-112.

Einarsson, E., Ma'ayeh, S., Svärd, S. G. 2016. An up-date on *Giardia* and giardiasis. Curr. Opin. Microbiol., 34, 47–52.

Fava, N. M. N., Silva, K. J. S., Snelling, W. J., Ternan, N. G., Dooley, J. S. G., Sabogal-Paz, L. P. 2021. Does each bead count? A reduced-cost approach for recovering waterborne protozoa from challenge water using immunomagnetic separation. J. Water Health. 19, 436-447.

Filice, F. P. 1952. Studies on the cytology and life history of a *Giardia* from the laboratory rat. University California Public Zoology, 57, 53–146.

Franco, R. M. B., Branco, N., Amaro, B. C. T., Neto, R. C., Fiuza, V. R. S. 2016. *Cryptosporidium* species and *Giardia* genotypes detected in surface water supply of Campinas, southeast Brazil, by molecular methods. J. Vet. Med. Res. 3, 1053-1059.

Freitas, B. L. S., Terin, U. C., Fava, N. M. N., Sabogal-Paz, L.P. 2021. Filter Media Depth and Its Effect on the Efficiency of Household Slow Sand Filter in Continuous Flow. J. Environ. Manage, 288, 112412.

Freitas, A. G. de, Bastos, R. K. X., Bevilacqua, P. D., Pádua, V. L., Pimenta, J. F. de P., Andrade, R. C. de. 2010. Recirculação de água de lavagem de filtros e perigos associados a protozoários. Eng. Sanit. e Ambient. 15, 37–46.

Frerichs, J. G., Joeris, K., Scheper, T., Konstantinov, K. 2001. *In situ* microscopy for on-line and in-line monitoring of cell populations in bioreactors. Animal cell technology: from target to market. ESACT Proceedings, 452-454.

Gonzalez, R., Woods, R. Digital image processing. 3rd Ed. Pearson Education, 2008. pp. 62-449.

Göröcs, Z., Baum, D., Song, F., de Haan, K., Koydemir, H.C., Yunzhe, Q., Cai, Z., Skandakumar, T., Peterman, S., Tamamitsu, M., Ozcan, A. 2020. Label-free detection of *Giardia lamblia* cysts using a deep learning-enabled portable imaging flow cytometer. Lab on a Chip, 20, 4404-4412.

Karanis, P., Kourenti, C., Smith, H. 2007. Waterborne transmission of protozoan parasites: a worldwide review of outbreaks and lessons learnt. J. Water Health. 5, 1–38.

Karanis, P., Schoenen, D., Seitz, H. M. 1996. *Giardia* and *Cryptosporidium* in backwash water from rapid sand filters used for drinking water production. Zentralblatt fur Bakteriol. 284, 107–114.

Koydemir, H. C., Gorocs, Z., Tseng, D., Cortazar, B., Feng, S., Chan, R. Y., Burbano, J., Mcleod, E., Ozcan, A. 2015. Rapid imaging, detection and quantification of *Giardia lamblia* cysts using mobile-phone based fluorescent microscopy and machine learning. Lab on a Chip, 15(5), 1284-1293.

Lindner, P., Krabichler, C., Rudolph, G., Scheper, T., Hitzmann, B. 2007. Application of in-situ-microscopy and digital image processing in yeast cultivations. 10th International IFAC Symposium on Computer Application in Biotechnology 1, Mexico.

Lüder, C., Lindner, P., Bulnes-Abundis, D., Lu, S. M., Lücking, T., Dörte, S., Scheper, T. 2014. *In situ* microscopy and MIR-spectroscopy as non-invasive optical sensors for cell cultivation process monitoring. Pharm. Bioprocess., 2(2), 157–166.

Marquard, D., Enders, A., Roth, G., Rinas, U., Scheper, T., Lindner, P. 2016. *In situ* microscopy for online monitoring of cell concentration in *Pichia pastoris* cultivations. J. Biotechnol., 20(234), 90-98.

MathWorks™. 2021. *Image Processing Toolbox (TM)*: *User´s Guide* (R2021b). Retrieved January 10, 2022 from www.mathworks.com/help/images/ref/regionprops.html.

McGrath, J. S., Honrado, C., Spencer, D., Horton, B., Bridle, H. L., Morgan, H. 2017. Analysis of parasitic protozoa at the single-cell level using microfluidic impedance cytometry. Sci. Rep. 7, 2601.

Mudanyali, O., Oztoprak, C., Tseng, D., Erlinger, A., Ozcan, A. 2010. Detection of waterborne parasites using field-portable and cost-effective lensfree microscopy. Lab on a Chip, 10, 2419-2423.

Rosado-García, F. M., Guerrero-Flórez, M., Karanis, G., Hinojosa, M. D.C., Karanis, P. 2017. Water-borne protozoa parasites: The Latin American perspective. Int. J. Hyg. Environ. Health, 220, 783–798.

Shrestha, R., Duwal, R., Wagle. S., Pokhrel, S., Giri, B., Neupane, B. B. 2020. A smartphone microscopic method for simultaneous detection of (oo)cysts of *Cryptosporidium* and *Giardia*. PLoS Negl. Trop. Dis., 8, 14(9): e0008560.

Soltys, Z., Orzylowska-Sliwinska, O., Zaremba, M., Orlowski, D., Piechota, M., Fiedorowicz, A., Janeczko, K., Oderfeld-Nowak, B. 2005. Quantitative morphological study of microglial cells in the ischemic rat brain using principal component analysis. J. Neurosci. Methods, 146, 50–60.

Suhr, H., Herkommer A. M. 2015. *In situ* microscopy using adjustment-free optics. J. Biomed. Opt., 20(11): 116007.

Suhr, H., Speil, P., Wehnert, G., Storhas, W. 1991. In-situ mikroskopiesonde und meβverfahren. offenlegungsschrift. Deutsches Pattentamt. DE 4032002 A1.

Suhr, H., Wehnert, G., Schneider, K., Bittner, C., Scholz, T., Geissler, P., Jähne, B., Scheper, T. 1995. *In situ* microscopy for on-line characterization of cell-populations in bioreactors, including cell-concentration measurements by depth from focus. Biotechnol. Bioeng., 47: 106-116.

Thompson, R. C. A., Olson, M. E., Zhu, G., Enomoto, S., Abrahamsen, M. S., Hijjawi, N. S. 2005. *Cryptosporidium* and cryptosporidiosis. Adv. Parasitol., 59, 77–158.

United States Environmental Protection Agency – USEPA. 2012. Method 1623.1 *Cryptosporidium* and *Giardia* in Water by Filtration/IMS/FA. EPA 816 – R-12-001. Office of Water (MS-140). Environmental Protection Agency, Washington, D.C.

Wei, N., You, J., Friehs, K., Flaschel, E., Nattkemper, T. W. 2007. An *in-situ* probe for on-line monitoring of cell density and viability on the basis of dark field microscopy in conjunction with image processing and supervised machine learning. Biotechnol. Bioeng., 97, 1489-1500.

Wiedemann, P., Guez, J. S., Wiegemann, H. B., Egner, F., Quintana, J. C., Asanza-Maldonado, D., Filipaki, M., Wilkesman, J., Schwiebert, C., Cassar, J. P., Dhulster, P., Suhr H. 2011. *In situ* microscopic cytometry enables noninvasive viability assessment of animal cells by measuring entropy states. Biotechnol. Bioeng., 108, 2884-2893.

Wu, T. F., Chen, Y. C., Wang, W. C., Kucknoor, A. S., Lin, C. J., Lo, Y. H., Yao, C. W., Lian, I. 2017. Rapid Waterborne Pathogen Detection with Mobile Electronics. Sensors (Basel, Switzerland), 17(6), 1348.